NANO LETTERS

pubs.acs.org/NanoLett Letter

Nanoscale TiO_2 Protection Layer Enhances the Built-In Field and Charge Separation Performance of GaP Photoelectrodes

Zihao Xu, Bingya Hou, Fengyi Zhao, Zhi Cai, Haotian Shi, Yawei Liu, Craig L. Hill, Djamaladdin G. Musaev, Matthew Mecklenburg, Stephen B. Cronin,* and Tianquan Lian*

Cite This: https://doi.org/10.1021/acs.nanolett.1c02257 Read Online

ACCESS | Metrics & More | Article Recommendations | Supporting Information

ABSTRACT: Nanoscale oxide layer protected semiconductor photoelectrodes show enhanced stability and performance for solar fuels generation, although the mechanism for the performance enhancement remains unclear due to a lack of understanding of the microscopic interfacial field and its effects. Here, we directly probe the interfacial fields at p-GaP electrodes protected by n-TiO_2 and its effect on charge carriers by transient reflectance spectroscopy. Increasing the TiO_2 layer thickness from 0 to 35 nm increases the field in the GaP depletion region, enhancing the rate and efficiency of interfacial electron transfer from the GaP to TiO_2 on the ps time scale as well as retarding interfacial recombination on the microsecond time scale. This study demonstrates a general method for providing a microscopic view of the photogenerated charge carrier's pathway and loss mechanisms from the bulk of the electrode to the long-lived separated charge at the interface that ultimately drives the photoelectrochemical reactions.

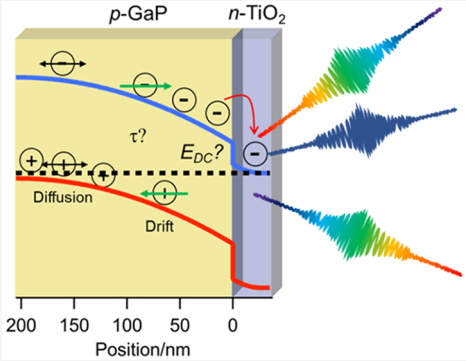

KEYWORDS: *Transient reflectance spectroscopy, GaP photoelectrode, oxide protection, charge carrier dynamics, interfacial charge separation, interfacial charge recombination, built-in field, Franz−Keldysh oscillations, FKO*

Downloaded via UNIV OF SOUTHERN CALIFORNIA on October 1, 2021 at 06:42:03 (UTC).
See https://pubs.acs.org/sharingguidelines for options on how to legitimately share published articles.

■ INTRODUCTION

In recent years, metal oxide passivation of semiconductors has emerged as an effective way to mitigate the long-standing problem of photocorrosion.[1−10] This has opened up the field of photocatalysis to a much broader range of semiconductor materials that were previously considered impractical due to their poor photochemical stability. This protection scheme has been demonstrated in Si,[5−7] GaAs,[5] GaP,[5,11,12] ZnO,[3] Fe_2O_3,[4] and InP[1,13] with TiO_2 films deposited by atomic layer deposition (ALD) using various precursors, including $TiCl_4$,[11,12] TDMAT (i.e., $[(CH_3)_2N]_4Ti$),[5,7,13] and titanium isopropoxide (i.e., $C_{12}H_{28}O_4Ti$).[1,13] TiO_2-coated III−V materials have been used for photocatalytic water splitting as well as CO_2 reduction.[12] A record high solar-to-hydrogen efficiency of 14% was achieved using TiO_2-coated InP nanopillars with a Ru catalyst.[1] Qiu et al. observed a reduction in the onset potential of TiO_2-coated GaP with increasing TiO_2 thickness from 1 to 10 nm and attributed this, at least in part, to the formation of a p−n junction that provides a built-in electric field to facilitate charge separation; however, no direct evidence of these fields or their dependence on TiO_2 thickness has been obtained.[11]

The built-in electric fields that are generated at the surface of semiconductors and at semiconductor−liquid interfaces provide the major driving force underlying photocatalytic processes.[14,15] While the built-in fields in solid-state photovoltaic systems are well understood, these have largely gone unstudied in photoelectrochemical systems. Figure 1 illustrates the band bending and depletion layer that arise from the formation of p−n junction between the p-type GaP single crystal and atomic layer deposited TiO_2. A built-in electric field (E_{DC}) is associated with this depletion region, as indicated in Figure 1, which separates the photoexcited electron−hole pairs, sweeping the minority carrier (electrons) to the surface and the majority carrier (holes) to the underlying GaP substrate. TiO_2 deposited by atomic layer deposition (ALD) is known to be doped n-type due to O-vacancies.[16,17] Therefore, passivating the surface of p-type GaP with an n-type TiO_2 layer with increasing thickness has been hypothesized to increase the depletion width and built-in field strength within the semiconductor.[4,5,11−13,18,19] This increases the effective volume of charge separation, which reduces electron−hole recombination and improves photocatalytic efficiency. However, direct probe of the effects of oxide layers on the built-in field strength and charge separation and recombination kinetics has been lacking. Although photogenerated carrier in semiconductor electrodes have been probed by transient optical absorption

Received: June 9, 2021

 © XXXX American Chemical Society

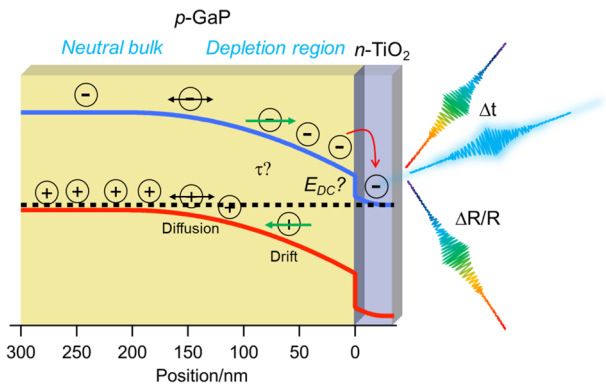

Figure 1. Schematic diagram illustrating the built-in field and surface depletion (i.e., charge separation) region in GaP coated with TiO_2. In this study, both the built-in field and the kinetics of charge carrier generation, transport, separation, and recombination are probed by transient reflectance spectroscopy.

spectroscopy,[2,20−37] such method lacks surface selectivity or sensitivity to allow unambiguous differentiation of bulk vs interfacial carriers and cannot directly measure built-in field strength. Because of their limited penetration depth, high energy probe techniques, such as ultrafast extreme ultraviolet (XUV) spectroscopy, X-ray absorption spectroscopy (XAS), X-ray absorption near-edge structure spectroscopy (XANES), and X-ray photoelectron spectroscopy (XPS), show unique advantages in identifying photogenerated carriers,[38−43] reaction specific sites,[44−46] and polaron[47−52] at the surface of photoactive semiconductor but require careful design to be applied *in situ* due to the strong absorbance of electrolyte.[53] Recent studies of $GaInP_2/TiO_2$,[18] $GaAs/TiO_2$,[54] and $SrTiO_3$[55,56] electrodes show that transient optical reflectance spectroscopy provides direct probe of interfacial field and is sensitive to surface carriers.

In this work, we report a transient reflectance spectroscopy (TRS) study of p-type GaP single crystal photoelectrodes

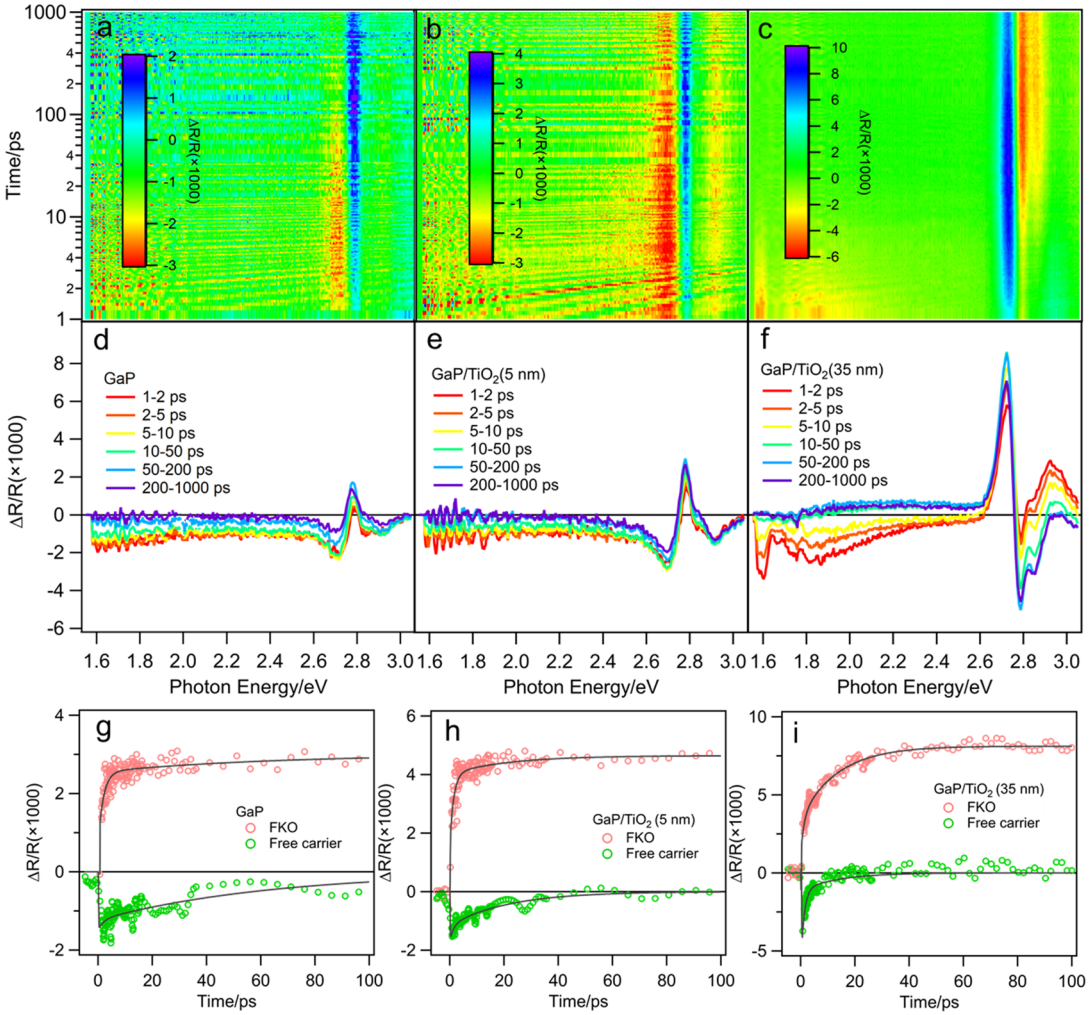

Figure 2. Transient reflection spectra and kinetics of GaP/TiO_2. 2D pseudocolor plots of the TR spectra of (a) bare GaP, (b) GaP/TiO_2(5 nm), and (c) GaP/TiO_2(35 nm) plotted as a function of delay time from 1 ps to 1 ns. Their corresponding average transient reflectance spectra in selected delay time windows are shown in (d)−(f), and the corresponding kinetics of free carrier signals probed at 1.8 eV (green circles) and FKO signals probed at ∼2.78 eV (pink circles) are plotted in (g)−(i). The FKO signal amplitudes are determined from the difference between the amplitudes at the peak (2.78 eV) and valley (2.70 eV) for (g) and (h) to remove the contribution of the free carrier signal. In (i), the amplitude of the free carrier signal is much smaller than the FKO signal and the peak amplitude at 2.72 eV is taken as the FKO signal amplitude. Also shown for comparison in (g)−(i) is the fit to multiexponential functions described in Supporting Information eq S2. The samples were excited at 400 nm (3.1 eV) with 0.16 mJ/cm^2 pulse energy density. The oscillations at 1.6−2.0 eV are noises from probe light.

https://doi.org/10.1021/acs.nanolett.1c02257
Nano Lett. XXXX, XXX, XXX−XXX

coated with TiO_2 of various thicknesses in order to explore the effect of enhanced electrostatic fields and the dynamics of photogenerated charge carriers at these p−n junctions. The shallow probe depth of this technique enables the selective observation of the surface charge carriers. These TR spectra show two main features that can be attributed to the photogenerated free carriers in GaP and separated carriers across the GaP/TiO_2 p−n junction. The observed kinetics of the free and separated carriers can be simulated based on a model that considers the built-in electrostatic field, photo-induced field, bulk recombination, charge carrier drift, diffusion, and transfer. This work provides a detailed microscopic view of the charge carrier's pathway from photoexcitation to the long-lived charge separation state that ultimately drives the photoelectrochemical reactions.

RESULTS AND DISCUSSION

To examine the effect of the TiO_2 layer thickness on photogenerated carrier dynamics, we compare three p-type GaP photoelectrodes with TiO_2 ALD layer thicknesses of 0 nm (bare GaP, referred to as GaP), 5 nm (GaP/TiO_2(5 nm)), and 35 nm (GaP/TiO_2(35 nm)). These GaP single crystal photoelectrodes are Zn doped with ∼6 × 10^{16} cm^{-3} dopant concentration and oriented along the (100) crystal surface. The TiO_2 layer is deposited by the atomic layer deposition (ALD) method. Further details of the photoelectrode preparation are provided in the Supporting Information. Similar photoelectrodes have been reported to actively photoreduce CO_2 and proton to produce solar fuels.[12] Because these photoelectrodes are opaque, transient reflectance spectroscopy (TRS) is used to probe the free carrier dynamics and transient electrostatic fields on ultrafast time scales.[18,20,55,57,58] In this study, the GaP samples were excited at 3.1 eV and probed at 1.6−3.1 eV. The pump penetration depth is ∼140 nm as determined by the relation $\lambda/(4\pi\kappa)$ (where κ is the imaginary part of the refractive index at the excitation wavelength λ), and the probe depth is 21−8 nm at 1.6−3.1 eV, given by $\lambda/(4\pi n)$ (where n is the real part of the refractive index at the probe wavelength).[59]

Figure 2a−c shows the 2D pseudocolor plots of the transient reflection spectra ($\Delta R/R$) of GaP, GaP/TiO_2(5 nm), and GaP/TiO_2(35 nm), respectively, at delay times from 0 to 1 ns after 400 nm excitation at a pulse energy density of 0.16 mJ/cm^2. The corresponding TR spectra at selected delay times are shown in Figure 2d−f. The TR spectra show two main features: (1) a broad negative feature (i.e., photoinduced decrease of reflectance) with decreasing amplitude at higher photon energy from 1.6 to 3 eV that can be assigned to photogenerated free carriers and (2) an oscillatory feature centered at the direct band gap of GaP at 2.78 eV, which is assigned to Franz−Keldysh oscillations (FKO),[59] as discussed below. From 0 to 100 ps, the amplitude of the free carrier signal decreases, while the amplitude of the FKO signal increases. This can be seen more clearly in Figure S2 and Figure 2g−i, in which the kinetics of free carrier signal at 1.8 eV and FKO signal at 2.78 eV are compared. The FKO kinetics can be fit with three exponential growth functions, as shown in Figure 2g−i and described in eq S2 and Table S1. A fast growth (<32 fs) is present for all three samples and two slow growths that are more pronounced in the GaP/TiO_2 (35 nm) sample. The comparison in Figure S2 shows that the decay of the free carrier signal agrees well with the growth of the FKO signal after ∼1 ps, suggesting that the decay of the free carriers in GaP leads to the formation of FKO. Indeed, for the same sample, the decay kinetics of the free carrier signal can be fit with two exponential functions with the same time constants as the slower growth components of the FKO signal. The fast (τ_0 < 32 fs) growth kinetics of the FKO signal is not observed in the corresponding decay of the free carrier amplitude because of the limited time resolution of the measurement, as discussed below. A comparison of the free carrier kinetics of GaP photoelectrodes with different TiO_2 layer thicknesses shows that the time constant (τ_2) for the slowest component decreases from 64 ps in bare GaP to 14 ps in GaP/TiO_2(35 nm). The same trend can be seen in the slow component of the FKO growth (Table S1), although they are less clearly shown because of the smaller contribution of this component to the overall FKO signal, especially in bare GaP and GaP/TiO_2(5 nm).

The broad negative feature is assigned to the reflectance change induced by photogenerated free carriers and is described by[60,61]

$$\frac{\Delta R}{R} = \frac{4n_0 \cos(\theta)}{({n_0}^2 - 1)[{n_0}^2 - \sin^2(\theta)]^{1/2}} \Delta n_{FC}(N,\mu) \tag{1}$$

According to the Drude model, the free carrier induced change in the reflective index, $\Delta n_{FC}(N,\mu)$, can be related to the photocarrier concentration (N) according to eq 2.[60,61]

$$\Delta n_{FC}(N,\mu) = -\frac{2\pi e^2}{n_0(\hbar\omega)^2}\frac{N}{\mu} \tag{2}$$

In eqs 1 and 2, n_0 is the amplitude of the complex refractive index. In the probe energy range of this study, the complex refractive index of GaP is dominated by the real part n, with a small imaginary part k (at 1.6 eV, n = 3.2, k = 0; at 3 eV, n = 4.1, k = 0.2).[59] μ is the reduced effective mass of the electron−hole pair, and θ is the incidence angle. According to eqs 1 and 2, the amplitude of this broad band signal should increase at lower frequency, which is in agreement with the observed results shown in Figure 2a−c. Similar free carrier induced reflectance changes have also been reported in other semiconductor photoelectrodes.[18,57]

The FKO signal is attributed to the change of GaP dielectric constant induced by the time-dependent electric field (E_{AC}) generated by the separated charges across the GaP/TiO_2 junction.[62,63] The photogenerated conduction band electrons and valence band holes in the GaP depletion region can recombine, diffuse (caused by the concentration gradient), and/or be transferred into TiO_2 and the bulk GaP photoelectrode (driven by the built-in electrical field in the depletion region within GaP), respectively.[54] The static built-in field in the dark (or the DC field, E_{DC}) is partially reduced (or screened) by the photogenerated field (E_{AC}) of the separated carriers, which leads to a change ($\Delta R/R$ signal) at the direct band gap transition as shown in Figure 3. Similar FKO signals have been observed in a recent TRS study of TiO_2 protected $GaInP_2$ photoelectrodes.[18,64] In the weak field (small E_{DC}), the FKO spectra can be simplified to a third derivative form.[62,63,65] In this regime, the light induced FKO signal is given by

$$\frac{\Delta R(\nu)}{R(\nu)} = \sum_{j=1}^{2} A_j \frac{e^2\hbar^2}{\mu_j} E_{AC}E_{DC}\mathrm{Re}[e^{i\phi_j}(h\nu - E_{gj} + i\Gamma_j)^{-m}] \tag{3}$$

https://doi.org/10.1021/acs.nanolett.1c02257
Nano Lett. XXXX, XXX, XXX−XXX

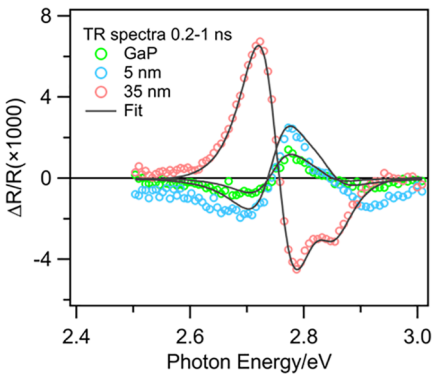

Figure 3. TR FKO spectra of GaP (green), GaP/TiO_2 (5 nm) (blue), and GaP/TiO_2 (35 nm) (red) averaged between 200 ps and 1 ns and their fits (black lines) to eq 3.

Further details of the derivation of this equation can be found in Supporting Information section 3.3. Here, j = 1, 2 for excitonic transitions involving light and heavy holes, μ_j is the effective mass of excitons, ϕ_j is the phase difference between the real and imaginary part of the refractive index, $h\nu$ is the photon energy, E_{gj} and Γ_j are the energy and width, respectively, of the exciton transitions. m = 2.5 for the direct transition critical point of GaP. As shown in Figure 3, the measured FKO spectra can be fit by eq 3 and the fitting parameters are listed in Table S2. According to eq 3, the FKO spectral shape is determined by the energy and width of the two excitonic transitions, and the FKO signal amplitude is proportional to the strength of the AC and DC fields, $\Delta R/R(\nu) \propto E_{DC}E_{AC}$.[62,63]

The time dependence of the FKO signal reflects how E_{AC} changes with time. At the direct band gap of GaP (2.78 eV), where the FKO signal is observed, the probe beam penetration depth is ∼10 nm. The FKO signal should be the average value within the probed region. For simplicity, we assume that the field strength can be approximately given by that at the GaP/TiO_2 interface. According to Gauss' law, the field strength at the GaP/TiO_2 interface is given by

$$(E_{AC})_{x=0} = \frac{\sigma}{\varepsilon\varepsilon_0} \tag{4}$$

In eq 4, σ is the total transferred charge across the GaP/TiO_2 interface per unit GaP surface area, ε is the relative permittivity of GaP (11.1),[16] and ε_0 is the vacuum permittivity. Thus, the FKO induced $\Delta R/R$ signal amplitude is linearly proportional to the concentration of the electrons that are transferred into TiO_2, providing a convenient probe of interfacial charge separation in the GaP/TiO_2 p−n junction. This model is consistent with the result shown in Figure 2g−i, in which the FKO growth agrees with free carrier decay, indicating that both signals depend linearly on carrier concentrations.

To provide a deeper understanding of the observed free and separated carrier kinetics, we simulate the temporal evolution of electron and hole spatial distributions in the GaP/TiO_2. This is done by numerically solving the coupled Poisson and transport equations. The simulation details can be found in Supporting Infomation section 3.4. Briefly, as shown in Figure 4a, the key processes include the following: recombination including electron−hole Shockley−Read−Hall recombination, surface recombination, and Auger recombination; transport of electrons and holes by diffusion and drift; electron transfer across the GaP/TiO_2 interface. The electric field is calculated as $E_{DC} - E_{AC}$, where E_{AC} is position-dependent as calculated from the Poisson equation and E_{DC} (also position dependent) is calculated from the depletion width w under the abrupt approximation.[66] From the numerical simulation, the density of electrons transferred from GaP to TiO_2 and E_{AC} are obtained, which yields the FKO kinetics, as shown in Figure 4b. In the simulation, the depletion width and the recombination rate constant are used as the fitting parameters to achieve the best fit of the measured kinetics.

As shown in Figure 4b, the model above provides a satisfactory fit to the FKO kinetics, accounting for both the slow and fast growth components of the FKO kinetics. At <1 ps, fast interfacial electron transfer from GaP to TiO_2 and fast electron−hole Auger recombination within the depletion region deplete the electrons near the GaP/TiO_2 interface, which gives rise to the nearly instantaneous rise of FKO signal shown in Figure 2g−i and Figure 4b. This also leads to a rapid decay of the free carrier population in GaP.

The slower decay of the free carrier signals and growth of the FKO signal at t > 1 ps are attributed to the diffusion and drift of electrons generated from the bulk GaP toward the interface. This trend is captured in the fit shown in Figure 4b. From bare GaP and GaP/TiO_2(5 nm) to GaP/TiO_2(35 nm), the contribution of the slow growth component to the measured FKO signal increases from 61% to 81.8% as

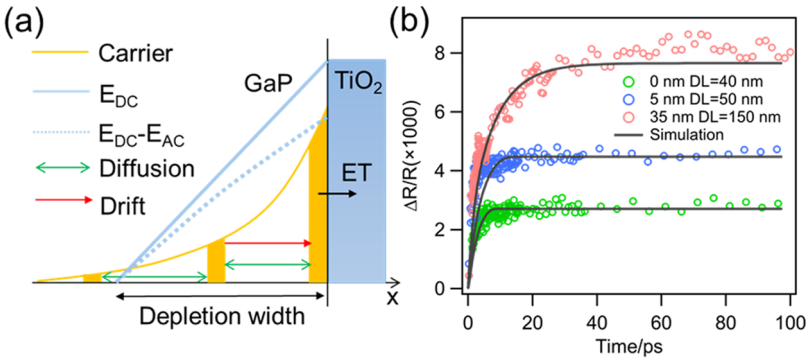

Figure 4. Simulation of photogenerated charge carrier kinetics. (a) Schematic diagram of the numerical simulation of a GaP/TiO_2 p−n junction. (b) Comparison of simulated kinetics of the electron transfer from the GaP to the TiO_2 (black line) and measured FKO kinetics (color circles, from Figure 2g−i) of bare GaP, GaP/TiO_2(5 nm), and GaP/TiO_2(35 nm). The depletion layer (DL) width used for simulation is shown in the legend.

https://doi.org/10.1021/acs.nanolett.1c02257
Nano Lett. XXXX, XXX, XXX−XXX

discussed above ($a_1 + a_2$, Table S1). To capture this trend in the simulated kinetics requires decreasing recombination rate k_r and increasing depletion width w from GaP to GaP/TiO_2(35 nm). For GaP/TiO_2(35 nm) where the slow component has the largest ratio, a large w (150 nm) is needed. This suggests that the larger depletion width, which reduces hole concentration near the surface, allows more charge carrier to survive the initial fast (~32 fs) Auger recombination phase and to be transported by the diffusion and drift processes to the p−n junction interface on a slower time scale. A comparison of the free carrier kinetics of GaP photoelectrodes with different TiO_2 layer thicknesses (Figure 2g−i, Figure S2) shows that the decay time constant decreases from 64 ps in bare GaP to 14 ps in GaP/TiO_2(35 nm), which can be attributed to faster drift times in the latter electrode caused by their larger built-in electric fields. Both the increased depletion width obtained from the fit and faster rate constant of the slow component provide direct evidence for the expected increase of built-in electric field in the junction as the TiO_2 layer thickness increases.

To understand the effect of built-in field strength on interfacial charge separation, we have also measured the charge separation kinetics as a function of excitation power density (detailed in Supporting Information section 3.5, Figure S4, and Table S5). The E_{AC} saturates at higher excitation power, indicating larger electron−hole recombination, consistent with the simulation results shown in Figure 4.

Interfacial Charge Recombination. The FKO kinetics at longer time scales (up to 100 μs) for GaP/TiO_2(5 nm) and GaP/TiO_2(35 nm) are shown in Figure 5. The kinetics for bare GaP are not shown because of their small signal amplitude and poor signal-to-noise ratio. The FKO signal decays on the 100 ps to 100 μs time scale and is assigned to the slow interfacial recombination of the separated electrons in TiO_2 and holes in GaP. The kinetics data are fitted to three exponential functions (eq S2), and the fitting parameters are listed in Table S4. The average amplitude weighted recombination time, calculated by eq S7, is 13.9 μs in the GaP/TiO_2(35 nm) and 6.0 μs in GaP/TiO_2(5 nm). The slower interfacial recombination in GaP/TiO_2(35 nm) is consistent with the increase of band bending and depletion width with thicker TiO_2. The larger band bending leads to a smaller hole density at the interface of GaP/TiO_2(35 nm), which reduces the interfacial recombination rate.

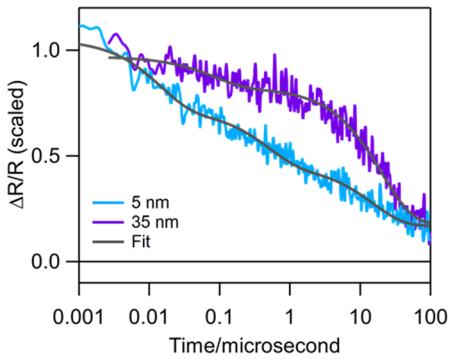

Figure 5. Comparison of the FKO decay kinetics of GaP/TiO_2(35 nm) and GaP/TiO_2(5 nm). FKO signal is monitored at 2.78 eV and measured with 3.1 eV excitation. Also shown by the black solid lines are fits to multiple exponential functions with fitting parameters listed in Table S5.

CONCLUSIONS

Transient reflectance spectroscopic measurements establish the role that amorphous TiO_2 layers play in controlling the charge separating fields and depletion regions at GaP/TiO_2 interfaces. The decay of photoexcited free carriers in GaP is observed as the decrease of a broad $\Delta R/R$ signal below the direct gap of GaP, and the extent of photodriven electron transfer across the GaP/TiO_2 junction can be followed by the growth of the Franz−Keldysh oscillation (FKO) signal at the GaP direct gap transition. Growth of the FKO signal shows an instantaneous phase with time constant of 32 fs and slower phase with time constants of ~2 and ~14 ps in GaP/TiO_2 (35 nm). Simulation of the kinetics of separated carriers and free carriers reveals that the fast phase is attributed to the initial fast interfacial electron transfer and bulk and surface recombination of photogenerated carriers in GaP. The slow phase is caused by the carriers within the bulk GaP and the depletion region away from the interface that undergoes relatively slower diffusion/drift. Over the 100 ps to 100 μs time scale, the FKO signal amplitude decays due to the slow interfacial recombination of the electrons in the TiO_2 with the holes in the GaP. Comparisons of GaP, GaP/TiO_2(5 nm), GaP/TiO_2(35 nm) show that the built-in field strength increases with TiO_2 thickness, which increases the rate and efficiency of initial charge separation across the GaP/TiO_2 interface by suppressing the charge recombination loss within GaP and slows down the interfacial recombination of separated electrons in the TiO_2 with holes in GaP. The reported TR technique directly probes the kinetics of photogenerated carriers in a photocatalytic p−n photoelectrode along their path from the initial generation in the bulk of GaP to the long-lived separated charges that ultimately drive photocatalytic reactions, enabling the direct identification of key loss pathways in semiconductor photoelectrodes.

ASSOCIATED CONTENT

Supporting Information

The Supporting Information is available free of charge at https://pubs.acs.org/doi/10.1021/acs.nanolett.1c02257.

Fitting function for FKO spectra and kinetics; continuity equation used in numerical simulation (PDF)

AUTHOR INFORMATION

Corresponding Authors

Stephen B. Cronin − *Departments of Electrical Engineering and Chemistry, University of South California, Los Angeles, California 90089, United States;* orcid.org/0000-0001-9153-7687; Email: scronin@usc.edu

Tianquan Lian − *Department of Chemistry, Emory University, Atlanta, Georgia 30322, United States;* orcid.org/0000-0002-8351-3690; Email: tlian@emory.edu

Authors

Zihao Xu − *Department of Chemistry, Emory University, Atlanta, Georgia 30322, United States;* orcid.org/0000-0003-0805-8533

Bingya Hou − *Departments of Electrical Engineering and Chemistry, University of South California, Los Angeles, California 90089, United States*

https://doi.org/10.1021/acs.nanolett.1c02257
Nano Lett. XXXX, XXX, XXX−XXX

Fengyi Zhao − *Department of Chemistry, Emory University, Atlanta, Georgia 30322, United States*
Zhi Cai − *Departments of Electrical Engineering and Chemistry, University of South California, Los Angeles, California 90089, United States*
Haotian Shi − *Departments of Electrical Engineering and Chemistry, University of South California, Los Angeles, California 90089, United States*
Yawei Liu − *Department of Chemistry, Emory University, Atlanta, Georgia 30322, United States*
Craig L. Hill − *Department of Chemistry, Emory University, Atlanta, Georgia 30322, United States;* orcid.org/0000-0002-5506-9588
Djamaladdin G. Musaev − *Department of Chemistry, Emory University, Atlanta, Georgia 30322, United States; Cherry L. Emerson Centre for Scientific Computation, Emory University, Atlanta, Georgia 30322, United States;* orcid.org/0000-0003-1160-6131
Matthew Mecklenburg − *Core Center of Excellence in Nano Imaging (CNI), University of South California, Los Angeles, California 90089, United States;* orcid.org/0000-0003-0581-4153

Complete contact information is available at:
https://pubs.acs.org/10.1021/acs.nanolett.1c02257

Notes

The authors declare no competing financial interest.

■ ACKNOWLEDGMENTS

This research was supported by the U.S. Department of Energy (DOE), Office of Science, Office of Basic Energy Sciences, Award DE-SC0019322 (B.H. and Z.X.) and Award DE-FG02-07ER-15906 (T.L., C.L.H., and D.G.M.).

■ REFERENCES

(1) Lee, M. H.; Takei, K.; Zhang, J. J.; Kapadia, R.; Zheng, M.; Chen, Y. Z.; Nah, J.; Matthews, T. S.; Chueh, Y. L.; Ager, J. W.; Javey, A. P-Type Inp Nanopillar Photocathodes for Efficient Solar-Driven Hydrogen Production. *Angew. Chem., Int. Ed.* **2012**, *51* (43), 10760−10764.
(2) Lin, Y.; Kapadia, R.; Yang, J.; Zheng, M.; Chen, K.; Hettick, M.; Yin, X.; Battaglia, C.; Sharp, I. D.; Ager, J. W.; Javey, A. Role of Tio2 Surface Passivation on Improving the Performance of P-Inp Photocathodes. *J. Phys. Chem. C* **2015**, *119* (5), 2308−2313.
(3) Appavoo, K.; Liu, M. Z.; Black, C. T.; Sfeir, M. Y. Quantifying Bulk and Surface Recombination Processes in Nanostructured Water Splitting Photocatalysts Via in Situ Ultrafast Spectroscopy. *Nano Lett.* **2015**, *15* (2), 1076−1082.
(4) Yang, X. G.; Liu, R.; Du, C.; Dai, P. C.; Zheng, Z.; Wang, D. W. Improving Hematite-Based Photoelectrochemical Water Splitting with Ultrathin Tio2 by Atomic Layer Deposition. *ACS Appl. Mater. Interfaces* **2014**, *6* (15), 12005−12011.
(5) Hu, S.; Shaner, M. R.; Beardslee, J. A.; Lichterman, M.; Brunschwig, B. S.; Lewis, N. S. Amorphous Tio_2 Coatings Stabilize Si, Gaas, and Gap Photoanodes for Efficient Water Oxidation. *Science* **2014**, *344* (6187), 1005−1009.
(6) Hwang, Y. J.; Boukai, A.; Yang, P. D. High Density N-Si/N-Tio2 Core/Shell Nanowire Arrays with Enhanced Photoactivity. *Nano Lett.* **2009**, *9* (1), 410−415.
(7) Chen, Y. W.; Prange, J. D.; Duhnen, S.; Park, Y.; Gunji, M.; Chidsey, C. E. D.; McIntyre, P. C. Atomic Layer-Deposited Tunnel Oxide Stabilizes Silicon Photoanodes for Water Oxidation. *Nat. Mater.* **2011**, *10* (7), 539−544.
(8) Park, S. M.; Barber, M. E. Thermodynamic Stabilities of Semiconductor Electrodes. *J. Electroanal. Chem. Interfacial Electrochem.* **1979**, *99* (1), 67−75.
(9) Frese, K. W.; Madou, M. J.; Morrison, S. R. Investigation of Photoelectrochemical Corrosion of Semiconductors 0.1. *J. Phys. Chem.* **1980**, *84* (24), 3172−3178.
(10) Frese, K. W.; Madou, M. J.; Morrison, S. R. Photoelectrochemical Corrosion of N-Gaas. *J. Electrochem. Soc.* **1980**, *127* (8), C370−C371.
(11) Qiu, J.; Zeng, G.; Pavaskar, P.; Li, Z.; Cronin, S. B. Plasmon-Enhanced Water Splitting on Tio_2-Passivated Gap Photocatalysts. *Phys. Chem. Chem. Phys.* **2014**, *16*, 3115.
(12) Zeng, G.; Qiu, J.; Pavaskar, P.; Li, Z.; Cronin, S. B. Co_2 Reduction to Methanol on Tio_2-Passivated Gap Photocatalysts. *ACS Catal.* **2014**, *4*, 3512.
(13) Lin, Y.; Kapadia, R.; Yang, J.; Zheng, M.; Chen, K.; Hettick, M.; Yin, X.; Battaglia, C.; Sharp, I. D.; Ager, J. W.; Javey, A. Role of Tio_2 Surface Passivation on Improving the Performance of *P*-Inp Photocathodes. *J. Phys. Chem. C* **2015**, *119*, 2308.
(14) Walter, M. G.; Warren, E. L.; McKone, J. R.; Boettcher, S. W.; Mi, Q.; Santori, E. A.; Lewis, N. S. Solar Water Splitting Cells. *Chem. Rev.* **2010**, *110* (11), 6446−6473.
(15) Lewis, N. S.; Nocera, D. G. Powering the Planet: Chemical Challenges in Solar Energy Utilization. *Proc. Natl. Acad. Sci. U. S. A.* **2006**, *103* (43), 15729−15735.
(16) Levinshtein, M. *Handbook Series on Semiconductor Parameters*; World Scientific, 1997; Vol. *1*, Chapter 5, pp 104−124.
(17) Aguirre, M. E.; Zhou, R.; Eugene, A. J.; Guzman, M. I.; Grela, M. A. Cu2o/Tio2 Heterostructures for Co2 Reduction through a Direct Z-Scheme: Protecting Cu2o from Photocorrosion. *Appl. Catal., B* **2017**, *217*, 485−493.
(18) Yang, Y.; Gu, J.; Young, J. L.; Miller, E. M.; Turner, J. A.; Neale, N. R.; Beard, M. C. Semiconductor Interfacial Carrier Dynamics Via Photoinduced Electric Fields. *Science* **2015**, *350* (6264), 1061−1065.
(19) Zeng, G.; Qiu, J.; Li, Z.; Pavaskar, P.; Cronin, S. B. Co2 Reduction to Methanol on Tio2-Passivated Gap Photocatalysts. *ACS Catal.* **2014**, *4* (10), 3512−3516.
(20) Huang, Z.; Lin, Y.; Xiang, X.; Rodríguez-Córdoba, W.; McDonald, K. J.; Hagen, K. S.; Choi, K.-S.; Brunschwig, B. S.; Musaev, D. G.; Hill, C. L.; Wang, D.; Lian, T. In Situ Probe of Photocarrier Dynamics in Water-Splitting Hematite (A-Fe2o3) Electrodes. *Energy Environ. Sci.* **2012**, *5* (10), 8923−8926.
(21) Selim, S.; Francàs, L.; García-Tecedor, M.; Corby, S.; Blackman, C.; Gimenez, S.; Durrant, J. R.; Kafizas, A. Wo3/Bivo4: Impact of Charge Separation at the Timescale of Water Oxidation. *Chemical Science* **2019**, *10* (9), 2643−2652.
(22) Kafizas, A.; Ma, Y.; Pastor, E.; Pendlebury, S. R.; Mesa, C.; Francàs, L.; Le Formal, F.; Noor, N.; Ling, M.; Sotelo-Vazquez, C.; Carmalt, C. J.; Parkin, I. P.; Durrant, J. R. Water Oxidation Kinetics of Accumulated Holes on the Surface of a Tio2 Photoanode: A Rate Law Analysis. *ACS Catal.* **2017**, *7* (7), 4896−4903.
(23) Ma, Y.; Mesa, C. A.; Pastor, E.; Kafizas, A.; Francàs, L.; Le Formal, F.; Pendlebury, S. R.; Durrant, J. R. Rate Law Analysis of Water Oxidation and Hole Scavenging on a Bivo4 Photoanode. *ACS Energy Letters* **2016**, *1* (3), 618−623.
(24) Le Formal, F.; Pastor, E.; Tilley, S. D.; Mesa, C. A.; Pendlebury, S. R.; Grätzel, M.; Durrant, J. R. Rate Law Analysis of Water Oxidation on a Hematite Surface. *J. Am. Chem. Soc.* **2015**, *137* (20), 6629−6637.
(25) Pendlebury, S. R.; Wang, X.; Le Formal, F.; Cornuz, M.; Kafizas, A.; Tilley, S. D.; Grätzel, M.; Durrant, J. R. Ultrafast Charge Carrier Recombination and Trapping in Hematite Photoanodes under Applied Bias. *J. Am. Chem. Soc.* **2014**, *136* (28), 9854−9857.
(26) Le Formal, F.; Pendlebury, S. R.; Cornuz, M.; Tilley, S. D.; Grätzel, M.; Durrant, J. R. Back Electron−Hole Recombination in Hematite Photoanodes for Water Splitting. *J. Am. Chem. Soc.* **2014**, *136* (6), 2564−2574.
(27) Ritchie, E. T.; Hill, D. J.; Mastin, T. M.; Deguzman, P. C.; Cahoon, J. F.; Atkin, J. M. Mapping Free-Carriers in Multijunction

Silicon Nanowires Using Infrared near-Field Optical Microscopy. *Nano Lett.* **2017**, *17* (11), 6591−6597.
(28) Lv, H.; Song, J.; Zhu, H.; Geletii, Y. V.; Bacsa, J.; Zhao, C.; Lian, T.; Musaev, D. G.; Hill, C. L. Visible-Light-Driven Hydrogen Evolution from Water Using a Noble-Metal-Free Polyoxometalate Catalyst. *J. Catal.* **2013**, *307*, 48−54.
(29) Hess, L. H.; Cooper, J. K.; Loiudice, A.; Jiang, C.-M.; Buonsanti, R.; Sharp, I. D. Probing Interfacial Energetics and Charge Transfer Kinetics in Semiconductor Nanocomposites: New Insights into Heterostructured Tio2/Bivo4 Photoanodes. *Nano Energy* **2017**, *34*, 375−384.
(30) Cooper, J. K.; Reyes-Lillo, S. E.; Hess, L. H.; Jiang, C.-M.; Neaton, J. B.; Sharp, I. D. Physical Origins of the Transient Absorption Spectra and Dynamics in Thin-Film Semiconductors: The Case of Bivo4. *J. Phys. Chem. C* **2018**, *122* (36), 20642−20652.
(31) Cating, E. E. M.; Pinion, C. W.; Christesen, J. D.; Christie, C. A.; Grumstrup, E. M.; Cahoon, J. F.; Papanikolas, J. M. Probing Intrawire, Interwire, and Diameter-Dependent Variations in Silicon Nanowire Surface Trap Density with Pump−Probe Microscopy. *Nano Lett.* **2017**, *17* (10), 5956−5961.
(32) Grumstrup, E. M.; Gabriel, M. M.; Pinion, C. W.; Parker, J. K.; Cahoon, J. F.; Papanikolas, J. M. Reversible Strain-Induced Electron−Hole Recombination in Silicon Nanowires Observed with Femtosecond Pump−Probe Microscopy. *Nano Lett.* **2014**, *14* (11), 6287−6292.
(33) Gabriel, M. M.; Grumstrup, E. M.; Kirschbrown, J. R.; Pinion, C. W.; Christesen, J. D.; Zigler, D. F.; Cating, E. E. M.; Cahoon, J. F.; Papanikolas, J. M. Imaging Charge Separation and Carrier Recombination in Nanowire P-I-N Junctions Using Ultrafast Microscopy. *Nano Lett.* **2014**, *14* (6), 3079−3087.
(34) Gabriel, M. M.; Kirschbrown, J. R.; Christesen, J. D.; Pinion, C. W.; Zigler, D. F.; Grumstrup, E. M.; Mehl, B. P.; Cating, E. E. M.; Cahoon, J. F.; Papanikolas, J. M. Direct Imaging of Free Carrier and Trap Carrier Motion in Silicon Nanowires by Spatially-Separated Femtosecond Pump−Probe Microscopy. *Nano Lett.* **2013**, *13* (3), 1336−1340.
(35) Klahr, B.; Gimenez, S.; Fabregat-Santiago, F.; Hamann, T.; Bisquert, J. Water Oxidation at Hematite Photoelectrodes: The Role of Surface States. *J. Am. Chem. Soc.* **2012**, *134* (9), 4294−4302.
(36) Zandi, O.; Hamann, T. W. Enhanced Water Splitting Efficiency through Selective Surface State Removal. *J. Phys. Chem. Lett.* **2014**, *5* (9), 1522−1526.
(37) Klahr, B.; Hamann, T. Water Oxidation on Hematite Photoelectrodes: Insight into the Nature of Surface States through in Situ Spectroelectrochemistry. *J. Phys. Chem. C* **2014**, *118* (19), 10393−10399.
(38) Ryland, E. S.; Zhang, K.; Vura-Weis, J. Sub-100 Fs Intersystem Crossing to a Metal-Centered Triplet in Ni(Ii)Oep Observed with M-Edge Xanes. *J. Phys. Chem. A* **2019**, *123* (25), 5214−5222.
(39) Jiang, C.-M.; Baker, L. R.; Lucas, J. M.; Vura-Weis, J.; Alivisatos, A. P.; Leone, S. R. Characterization of Photo-Induced Charge Transfer and Hot Carrier Relaxation Pathways in Spinel Cobalt Oxide (Co3o4). *J. Phys. Chem. C* **2014**, *118* (39), 22774−22784.
(40) Baker, L. R.; Jiang, C.-M.; Kelly, S. T.; Lucas, J. M.; Vura-Weis, J.; Gilles, M. K.; Alivisatos, A. P.; Leone, S. R. Charge Carrier Dynamics of Photoexcited Co3o4 in Methanol: Extending High Harmonic Transient Absorption Spectroscopy to Liquid Environments. *Nano Lett.* **2014**, *14* (10), 5883−5890.
(41) Lin, M.-F.; Verkamp, M. A.; Leveillee, J.; Ryland, E. S.; Benke, K.; Zhang, K.; Weninger, C.; Shen, X.; Li, R.; Fritz, D.; Bergmann, U.; Wang, X.; Schleife, A.; Vura-Weis, J. Carrier-Specific Femtosecond Xuv Transient Absorption of Pbi2 Reveals Ultrafast Nonradiative Recombination. *J. Phys. Chem. C* **2017**, *121* (50), 27886−27893.
(42) Cooper, J. K.; Gul, S.; Toma, F. M.; Chen, L.; Liu, Y.-S.; Guo, J.; Ager, J. W.; Yano, J.; Sharp, I. D. Indirect Bandgap and Optical Properties of Monoclinic Bismuth Vanadate. *J. Phys. Chem. C* **2015**, *119* (6), 2969−2974.
(43) Cooper, J. K.; Gul, S.; Toma, F. M.; Chen, L.; Glans, P.-A.; Guo, J.; Ager, J. W.; Yano, J.; Sharp, I. D. Electronic Structure of Monoclinic Bivo4. *Chem. Mater.* **2014**, *26* (18), 5365−5373.
(44) Ash, R.; Zhang, K.; Vura-Weis, J. Photoinduced Valence Tautomerism of a Cobalt-Dioxolene Complex Revealed with Femtosecond M-Edge Xanes. *J. Chem. Phys.* **2019**, *151* (10), 104201.
(45) Chen, L.; Alarcón-Lladó, E.; Hettick, M.; Sharp, I. D.; Lin, Y.; Javey, A.; Ager, J. W. Reactive Sputtering of Bismuth Vanadate Photoanodes for Solar Water Splitting. *J. Phys. Chem. C* **2013**, *117* (42), 21635−21642.
(46) McDowell, M. T.; Lichterman, M. F.; Spurgeon, J. M.; Hu, S.; Sharp, I. D.; Brunschwig, B. S.; Lewis, N. S. Improved Stability of Polycrystalline Bismuth Vanadate Photoanodes by Use of Dual-Layer Thin Tio2/Ni Coatings. *J. Phys. Chem. C* **2014**, *118* (34), 19618−19624.
(47) Biswas, S.; Wallentine, S.; Bandaranayake, S.; Baker, L. R. Controlling Polaron Formation at Hematite Surfaces by Molecular Functionalization Probed by Xuv Reflection-Absorption Spectroscopy. *J. Chem. Phys.* **2019**, *151* (10), 104701.
(48) Husek, J.; Cirri, A.; Biswas, S.; Baker, L. R. Surface Electron Dynamics in Hematite (A-Fe2o3): Correlation between Ultrafast Surface Electron Trapping and Small Polaron Formation. *Chemical Science* **2017**, *8* (12), 8170−8178.
(49) Biswas, S.; Husek, J.; Londo, S.; Baker, L. R. Ultrafast Electron Trapping and Defect-Mediated Recombination in Nio Probed by Femtosecond Extreme Ultraviolet Reflection−Absorption Spectroscopy. *J. Phys. Chem. Lett.* **2018**, *9* (17), 5047−5054.
(50) Cirri, A.; Husek, J.; Biswas, S.; Baker, L. R. Achieving Surface Sensitivity in Ultrafast Xuv Spectroscopy: M2,3-Edge Reflection−Absorption of Transition Metal Oxides. *J. Phys. Chem. C* **2017**, *121* (29), 15861−15869.
(51) Biswas, S.; Husek, J.; Baker, L. R. Elucidating Ultrafast Electron Dynamics at Surfaces Using Extreme Ultraviolet (Xuv) Reflection−Absorption Spectroscopy. *Chem. Commun.* **2018**, *54* (34), 4216−4230.
(52) Biswas, S.; Husek, J.; Londo, S.; Fugate, E. A.; Baker, L. R. Identifying the Acceptor State in Nio Hole Collection Layers: Direct Observation of Exciton Dissociation and Interfacial Hole Transfer across a Fe2o3/Nio Heterojunction. *Phys. Chem. Chem. Phys.* **2018**, *20* (38), 24545−24552.
(53) Favaro, M.; Yang, J.; Nappini, S.; Magnano, E.; Toma, F. M.; Crumlin, E. J.; Yano, J.; Sharp, I. D. Understanding the Oxygen Evolution Reaction Mechanism on Coox Using Operando Ambient-Pressure X-Ray Photoelectron Spectroscopy. *J. Am. Chem. Soc.* **2017**, *139* (26), 8960−8970.
(54) Chen, X.; Pekarek, R. T.; Gu, J.; Zakutayev, A.; Hurst, K. E.; Neale, N. R.; Yang, Y.; Beard, M. C. Transient Evolution of the Built-in Field at Junctions of Gaas. *ACS Appl. Mater. Interfaces* **2020**, *12* (36), 40339−40346.
(55) Chen, X.; Choing, S. N.; Aschaffenburg, D. J.; Pemmaraju, C. D.; Prendergast, D.; Cuk, T. The Formation Time of Ti−O· and Ti−O·−Ti Radicals at the N-Srtio3/Aqueous Interface During Photocatalytic Water Oxidation. *J. Am. Chem. Soc.* **2017**, *139* (5), 1830−1841.
(56) Chen, X.; Aschaffenburg, D. J.; Cuk, T. Selecting between Two Transition States by Which Water Oxidation Intermediates Decay on an Oxide Surface. *Nature Catalysis* **2019**, *2* (9), 820−827.
(57) Zhang, C.; Fan, Y.; Huang, X.; Zhang, K. H. L.; Beard, M. C.; Yang, Y. Hot-Carrier Transfer at Photocatalytic Silicon/Platinum Interfaces. *J. Chem. Phys.* **2020**, *152* (14), 144705.
(58) Yang, Y.; Yan, Y.; Yang, M.; Choi, S.; Zhu, K.; Luther, J. M.; Beard, M. C. Low Surface Recombination Velocity in Solution-Grown Ch3nh3pbbr3 Perovskite Single Crystal. *Nat. Commun.* **2015**, *6* (1), 7961.
(59) Jellison, G. E. Optical Functions of Gaas, Gap, and Ge Determined by Two-Channel Polarization Modulation Ellipsometry. *Opt. Mater.* **1992**, *1* (3), 151−160.

https://doi.org/10.1021/acs.nanolett.1c02257
Nano Lett. XXXX, XXX, XXX−XXX

(60) Sabbah, A. J.; Riffe, D. M. Femtosecond Pump-Probe Reflectivity Study of Silicon Carrier Dynamics. *Phys. Rev. B: Condens. Matter Mater. Phys.* **2002**, *66* (16), 165217.
(61) Prabhu, S. S.; Vengurlekar, A. S. Dynamics of the Pump-Probe Reflectivity Spectra in Gaas and Gan. *J. Appl. Phys.* **2004**, *95* (12), 7803−7812.
(62) Shen, H.; Dutta, M. Franz−Keldysh Oscillations in Modulation Spectroscopy. *J. Appl. Phys.* **1995**, *78* (4), 2151−2176.
(63) Shen, H.; Pollak, F. H. Generalized Franz-Keldysh Theory of Electromodulation. *Phys. Rev. B: Condens. Matter Mater. Phys.* **1990**, *42* (11), 7097.
(64) Yang, Y.; Li, J.; Lin, L.; Peng, X. An Efficient and Surface-Benign Purification Scheme for Colloidal Nanocrystals Based on Quantitative Assessment. *Nano Res.* **2015**, *8* (10), 3353−3364.
(65) Hall, D. J.; Hosea, T. J. C.; Lancefield, D. Airy Function Analysis of Franz−Keldysh Oscillations in the Photoreflectance Spectra of In1−Xgaxasyp1−Y Layers. *J. Appl. Phys.* **1997**, *82* (6), 3092−3099.
(66) Dimitrijev, S. *Principles of Semiconductor Devices*, 2nd ed.; Oxford University Press: New York, 2012; p xix, 620 pp.

https://doi.org/10.1021/acs.nanolett.1c02257
Nano Lett. XXXX, XXX, XXX−XXX